Power Factor Control of Large Doubly-Fed Reluctance Wind Generators

Jude K. Obichere, Milutin Jovanovic and Sul Ademi

Abstract – **This paper deals with vector control (VC) of an emerging brushless doubly-fed reluctance (BDFRG) technology for large-scale wind turbines. The BDFRG has been receiving promising attention due to its low operation and maintenance costs afforded by the use of partially-rated power electronics, and the high reliability of brushless construction, while offering performance competitive to its traditional slip-ring counterpart, the doubly-fed induction generator (DFIG). A robust VC control scheme has been developed for a custom-designed BDFRG fed from a conventional 'back-to-back' IGBT converter. The preliminary studies have evaluated the algorithm under the maximum power factor control (MPFC) conditions which allow the improved efficiency of the generator-converter set and the entire wind energy conversion systems (WECS).**

Index Terms – **Doubly-Fed Machines, Power Factor Control, Vector Control, Wind Power**

I. INTRODUCTION

THE brushless doubly-fed generator (BDFG) has been considered as a viable replacement to the traditional DFIG for wind turbines [1]-[7]. In these applications, where only a limited variable speed capability is required (e.g. typically, in a 2:1 range or so [1], [4], [8]), the BDFG should retain the DFIG economic benefits of using a relatively smaller inverter (e.g. around 25% of the machine rating), but with higher reliability and maintenance-free operation afforded by the absence of brush gear [9], [10].

The BDFG has two standard stator windings of different applied frequencies and pole numbers, unlike the DFIG. The primary (power) winding is grid-connected, and the secondary (control) winding is normally supplied from a bi-directional power converter. A BDFG reluctance type (Fig. 1), the brushless doubly-fed reluctance generator (BDFRG) [1]–[4], appears to be more attractive than its 'nested' cage rotor form, the brushless doubly-fed induction generator (BDFIG) [5]–[7], [11], [12]. This preference has been mainly attributed to the prospect for higher efficiency [2] and simpler control associated with the cage-less reluctance rotor [14]. However, the BDFG rotor must have half the total number of stator poles to provide the rotor position

dependent magnetic coupling between the stator windings required for the machine torque production [3].

With the recent introduction of the grid codes [15], another important BDFG merit is the superior low-voltage-fault-ride-through (LVFRT) capability to the DFIG [16]–[18]. It has been shown that owing to the larger leakage inductances and lower fault current levels, the LVFRT of the BDFIG may be accomplished safely without a crowbar circuitry [15], [19]. These potential LVFRT performance advantages over the DFIG can be carried over to the BDFRG featuring the leakage reactance values of the same order as the BDFIG.
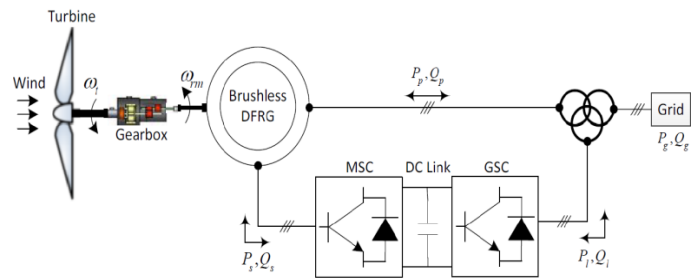

Fig. 1. Typical BDFRG drive set-up of variable speed WECS.

Various control algorithms have been developed for the BDFRG including scalar control [1], [21], vector control (VC) [1], [13], [21], [28], direct torque control [21], [22], torque and reactive power control [23], direct power control [24], sliding mode power control [25], field-oriented control [28], and even non-linear Lyapunov control theory [8]. Although a comparative analysis of some of these control methods has been partly made in [21], [28] (and more detailed for the DFIG in [16], [20]), it is interesting that there is very little reported specifically on Power Factor Control (PFC) of the BDFRG being of utmost importance for generator applications. In the BDFRG, the 'VC' term is commonly referred to as the primary winding voltage control, by analogy to the stator voltage control of the DFIG. With a proper selection of the reference frames and careful tuning of the dedicated PI controllers, a very good potential and dynamic response of the VC scheme has been demonstrated without knowledge of any machine parameters. The VC performance is examined using the maximum power factor control (MPFC) strategy [23], [24] on a large, custom-built 2 MW BDFRG [4]. This control objective has been considered because of the achievable efficiency gain at unity line power factor. Extensive realistic simulation results taking into account the usual practical effects (e.g. transducers' DC offset, noise in measurements,

and a PWM power converter model) are presented to support the discussions in this paper.

II. MODELING AND OPERATING PRINCIPLES

The dynamic model of the BDFRG in arbitrary rotating reference frames, assuming motoring convention, can be represented using standard complex notation as [3]:

$$
\left.
\begin{aligned}
\mathbf{v}_p &= R_p\mathbf{i}_p + \frac{d\lambda_p}{dt} = R_p\mathbf{i}_p + \frac{d\lambda_p}{dt}\big|\theta_{p\,const} + j\omega_p\lambda_p \\
\mathbf{v}_s &= R_s\mathbf{i}_s + \frac{d\lambda_s}{dt} = R_s\mathbf{i}_s + \frac{d\lambda_s}{dt}\big|\theta_{s\,const} + j\omega_s\lambda_s \\
\lambda_p &= \underbrace{L_p i_{pd} + L_{ps}i_{sd}}_{\lambda_{pd}} + j.\underbrace{(L_p i_{pq} - L_{ps}i_{sq})}_{\lambda_{pq}} \\
\lambda_s &= \lambda_{sd} + j.\lambda_{sq} = \sigma L_s\mathbf{i}_s + \underbrace{\frac{L_{ps}}{L_p}\lambda_p^*}_{\lambda_{ps}}
\end{aligned}
\right\} \quad (1)
$$

where the primary and secondary winding are denoted by the subscripts 'p' and 's' respectively, $\sigma = 1 - \frac{L_{ps}^2}{L_p L_s}$ is the leakage factor, and λ_{ps} is the primary flux linking the secondary winding (i.e. the mutual flux linkage).

The fundamental angular velocity and torque relationships for the machine with p_r rotor poles and $\omega_{p,s} = 2\pi f_{p,s}$ applied angular frequencies to the respective 2p-pole primary and 2q-pole secondary windings are [3]:

$$
\omega_{rm} = \frac{\omega_p + \omega_s}{p_r} \leftrightarrow n_{rm} = 60.\frac{f_p + f_s}{p_r} \quad (2)
$$

$$
T_e = \frac{3p_r}{2}(\lambda_{psd}i_{sq} - \lambda_{psq}i_{sd}) \quad (3)
$$

$$
T_a = J.\frac{d\omega_{rm}}{dt} = T_e - T_L(\omega_{rm}) - F.\omega_{rm} \quad (4)
$$

Notice that $\omega_s > 0$ for 'super-synchronous' operation, and $\omega_s < 0$ at sub-synchronous speeds (i.e. an opposite phase sequence of the secondary to the primary winding) in (2) where $\omega_{syn} = \frac{\omega_p}{p_r}$ is the synchronous speed (for $\omega_s = 0$ i.e. a DC secondary) as with a $2p_r$-pole wound rotor synchronous turbo-machine. It is also worth mentioning that all the ω_p rotating vectors in the primary voltage/flux equations in (1) are in ω_p frame, whilst the corresponding secondary counterparts, including the λ_{ps} components in (3), are stationary in $p_r\omega_{rm} - \omega_p = \omega_s$ frame [3]. Given that λ_p and λ_{ps} in (3) are approximately constant by the primary winding grid connection, torque control can obviously be achieved through the secondary dq currents in the ω_s rotating frame.

Using (2), one can derive the mechanical power equation indicating individual contributions of each BDFRG winding:

$$
P_m = T_e.\omega_{rm} = \underbrace{\frac{T_e.\omega_p}{p_r}}_{P_p} + \underbrace{\frac{T_e.\omega_s}{P_r}}_{P_s} = P_p.\left(1 + \frac{\omega_s}{\omega_p}\right) \quad (5)
$$

The machine operating mode is determined by the power flow in the primary winding i.e. to the grid for the generating ($T_e < 0$) regime under consideration, while the secondary winding can either take or deliver real power (P_s) subject to its phase sequence i.e. the ω_s sign; the BDFRG would absorb (produce) $P_s > 0$ at sub- or super-synchronous speeds.

III. CONTROLLER DESIGN

The detailed BDFRG system layout with a generic controller design is presented in Fig. 2. A standard phase-locked-loop (PLL) algorithm, readily available in the *Simulink* library, has been used to retrieve the stationary α-β frame angular positions (θ/θ_p) of the primary voltage/flux vectors from the measured voltages and/or currents. Furthermore, a conventional vector controller with space-vector PWM of the active rectifier has been implemented for control of DC link voltage and unity line power factor [24], [27]-[32]. The primary real (P) and reactive (Q) power calculations are reference frame invariant and have been done using the stationary frame voltages ($v_{\alpha\beta}$) and currents ($i_{\alpha\beta}$) to avoid unnecessary conversions into their rotating d_s-q_s equivalents, and the use of time-consuming trigonometric functions, allowing so the higher control rates and superior performance in practice. The Q reference is often set to zero (Q* = 0) for the unity primary power factor but can be any other value of interest for a given real power setting (P*) in power control mode, or the desired angular velocity ω_{rm}^* in variable speed systems. For example, either P* or ω_{rm}^* may correspond to the Maximum Power Point Tracking (MPPT) of a wind turbine [1], [8] while Q* was chosen to optimize efficiency of the WECS in this paper.
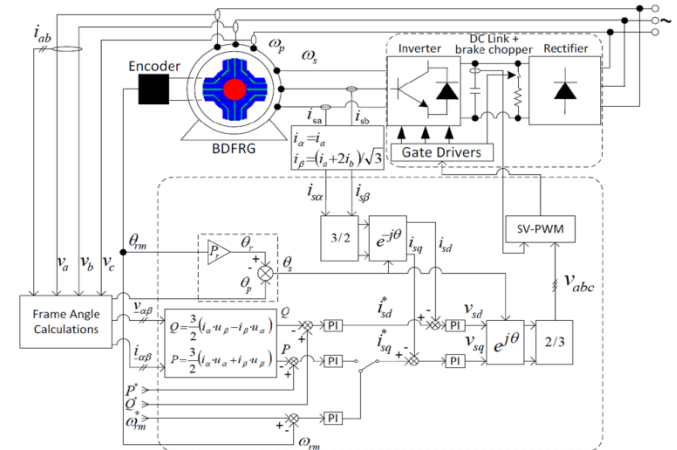

Fig. 2. Structural diagram of the BDFRG drive set-up.

IV. VOLTAGE CONTROL (VC)

The control form expressions can be derived from the BDFRG space-vector model (1) in the natural reference frames, ω_p (i.e. d_p-d_q for the primary winding) and ω_s (i.e. d_s-q_s for secondary winding) rotating frames (Fig. 3), where the respective vector components appear as DC quantities. Substituting for $\mathbf{i}_p$ from the λ_p equation of (1) into $\mathbf{S}_p = \frac{3}{2}\mathbf{v}_p\mathbf{i}_p^*$ would lead to the following relationships for the primary mechanical and reactive power:

$$
P_p = \frac{3}{2}\omega_p(\lambda_{psd}i_{sq} - \lambda_{psq}i_{sd}) \quad (6)
$$

$$
Q_p = \frac{3}{2}\omega_p\left(\frac{\lambda_p^2}{L_p} - \lambda_{psd}i_{sd} - \lambda_{psq}i_{sq}\right) \quad (7)
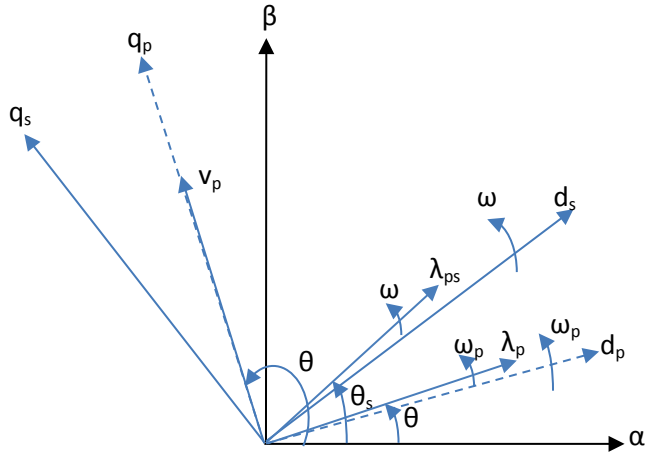$$

Fig. 3. Identification of primary voltage and flux vectors in a stationary α-β reference frame.

A trade-off of the machine parameter independence is that VC of P_p and Q_p is coupled as both the i_{sd} and i_{sq} secondary current components appear in (6) and (7). The level of this cross-coupling can be reduced by aligning the q_p-axis of the reference frame to the primary voltage vector as shown in Fig. 3. In this case the primary flux vector (λ_p), would be phase-shifted ahead of the corresponding d_p-axis depending on the winding resistance values which are getting smaller with larger machines. Therefore, for the frame alignment choice as in Fig. 3, $\lambda_{p_{sd}} \gg \lambda_{p_{sq}}$ i.e. $\lambda_{p_{sd}} \approx \lambda_{ps}$ so that the approximations of (6) and (7) become:

$$P_p \approx \frac{3}{2} \omega_p \lambda_{ps} i_{sq} = \frac{3}{2} \frac{L_{ps}}{L_p} \omega_p \lambda_p i_{sq} \qquad (8)$$

$$Q_p \approx \frac{3}{2} \frac{\omega_p \lambda_p^2}{L_p} - \frac{3}{2} \omega_p \lambda_{ps} i_{sd} \qquad (9)$$

$$= \frac{3}{2} \frac{\omega_p \lambda_p}{L_p} (\lambda_p - L_{ps} i_{sd}) = \frac{3}{2} \omega_p \lambda_p i_{pd} \qquad (10)$$

The P_p vs i_{sq} and Q_p vs i_{sd} functions above are nearly linear, which justifies the use of PI controllers in Fig. 2. Therefore, all inductance variations in (8)-(10) can be effectively taken care of by optimal tuning of the PI gains so their prior knowledge is not required for control purposes.

V. MPF OPERATION OF BDFRG WIND TURBINE

The preliminary performance of the VC scheme in Fig. 2 has been assessed using the parameters of a large-scale BDFRG [4],[29] in Table I for simulation studies. In order to make the simulations as realistic as possible, the following actions have been taken and/or assumptions made: (i) The power electronic models from the *SimPowerSystems* toolbox have been implemented; (ii) High-frequency uncorrelated white noise and unknown slowly varying DC offset have been superimposed to the ideal signals to account for practical effects of the measurement noise and current/voltage transducers errors; (iii) Finally, the rotor position and speed information has been provided by a shaft sensor.

In a typical WECS, the turbine torque on the generator side of the gear-box for the maximum wind energy

extraction in the base speed region (i.e. between the minimum 'cut-in', u_{min}, and the rated wind speed, u_r), can be represented as [1], [8]:

$$T_{opt} = \frac{A.\rho.C_p(\lambda_{opt},\gamma).R^3}{2.g^3.\lambda_{opt}^3} . \omega_{rm}^2 = K_{opt} . \omega_{rm}^2 \qquad (11)$$

where ρ is the air density, $C_p(\lambda,\gamma)$ is the power coefficient (i.e. the maximum turbine efficiency as $\lambda = \lambda_{opt}$ in this case), $\lambda_{opt} = \frac{R\omega_t}{u}$ is the optimum tip speed ratio for a given wind speed u, ω_t is the turbine rotor angular velocity, γ is the pitch angle (normally fixed to zero to maximise C_p), R the radius of the circular swept area (A = πR^2), and g = $\frac{\omega_{rm}}{\omega_t}$ is the gear ratio. The shaft torque-speed profile in (4) is of the same form as (11):

$$T_L = -\frac{P_r}{\omega_r} . \left(\frac{n_{rm}}{n_{max}}\right)^2 \approx -19. \left(\frac{n_{rm}}{1000}\right)^2 \text{ kNm} \qquad (12)$$

TABLE 1
THE BDFRG DESIGN SPECIFICATIONS

Symbol	Quantity	Values & Units
J	Rotor inertia	3.8 kgm^2
R_p	Primary resistance	0.0375 Ω
R_s	Secondary resistance	0.0575 Ω
L_p	Primary inductance	1.17 mH
L_s	Secondary inductance	2.89 mH
L_{ps}	Mutual inductance	0.98 mH
p_r	Rotor poles	4
P	Primary power	2 MW
n_r	Rated speed	1000 rev/min
$I_{p,s}$	Stator currents	1.5 kA rms
V_p	Primary voltage	690 V rms
f_p	Supply frequency	50 Hz
Y/Y	Winding connections	-
p/q	Stator poles	6/2

VI. SIMULATION RESULTS

The simulation results in Figs. 4-7 have been produced by running the control algorithms in Fig. 2 at 5 kHz switching rate for the IGBT converter. The DC link voltage has been maintained at ≈ 1200 V by the PWM rectifier (i.e. the line-side bridge) supplied at 690 V, 50 Hz. The reference speed trajectory is set as a steep ramp signal suited for dynamically not very demanding wind power applications even under extreme turbulent wind conditions.

The top plots in Fig. 4 show the excellent speed tracking with no overshoot following the start-up period in both super- and sub-synchronous modes of the BDFRG over the limited speed range of 600-900 rpm. The primary electrical power (P) and electro-magnetic torque (T_e) curves reflect (12) for the specific speed settings. Except for a difference in losses, and considering that $\omega_p \approx$ const, P and T_e are directly related as follows from (5) and (6) which explains a close resemblance in their shape. The T_e deviations from the desired profile during the speed transients refer to the acceleration or deceleration torque term in (4) depending on whether the machine is to speed-up ($T_a > 0$) or slow-down

($T_a < 0$). The reasonably accurate and smooth $Q_p \approx 0$ control can be observed to be little affected by the variable speed dependent loading disturbances, which means that the maximum power factor control (MPFC) conditions have been largely met. Note that the outer PI speed control loop is required to ensure effective variable speed operation at optimum tip-speed ratio.
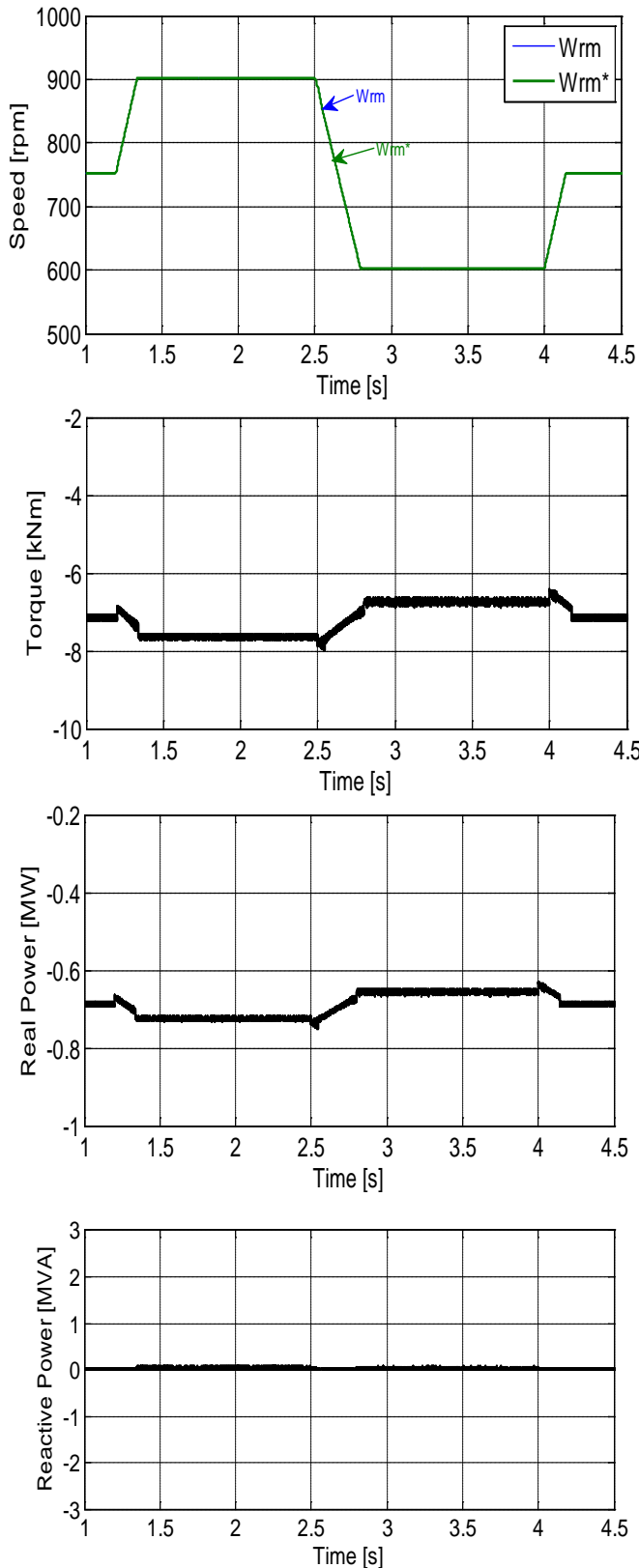

Fig. 4. MPF performance of the BDFRG in a limited range around synchronous speed (750 rpm).
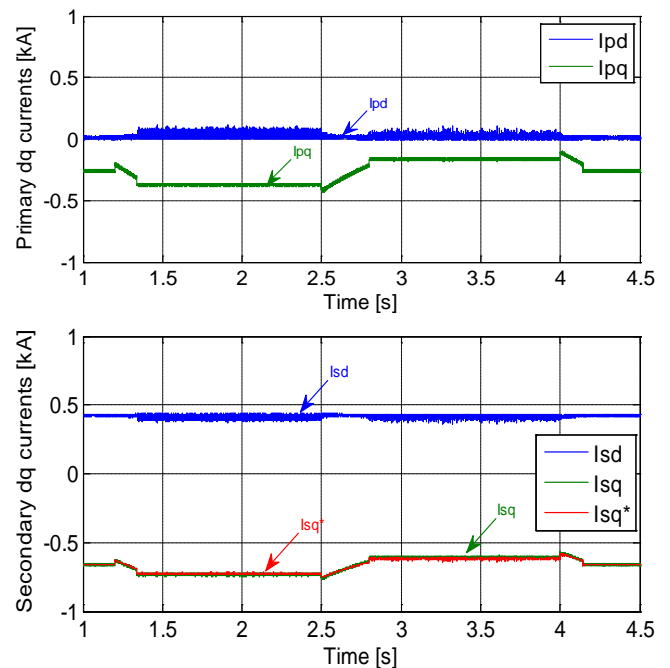

Fig. 5. MPF responses of the BDFRG current components in the corresponding rotating reference frames.
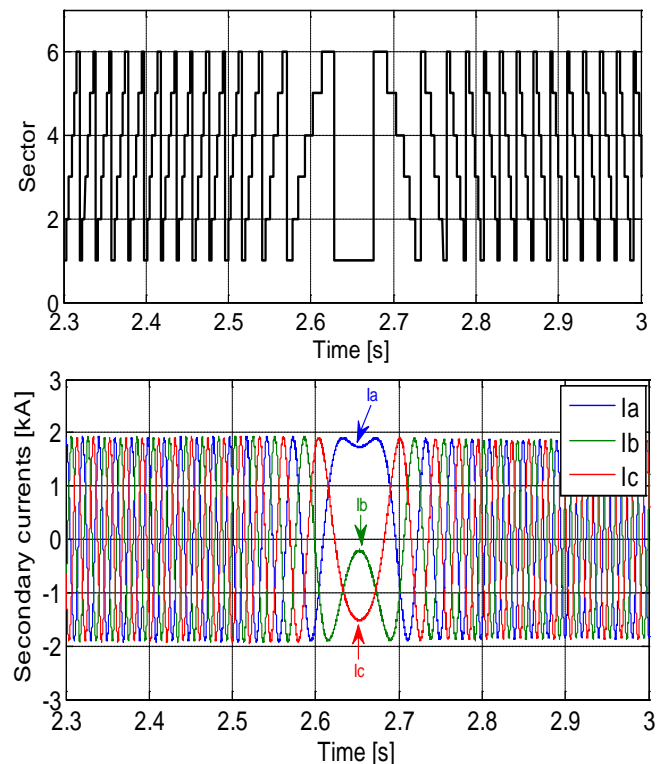

Fig. 6. BDFRG secondary voltage positions and secondary current waveforms showing a phase sequence reversal during the speed mode transition at unity power factor.

The secondary ($i_{sd,q}$) and primary ($i_{pd,q}$) current waveforms in Fig. 5 show no transient over-currents as the PI regulators do not need to be saturated to allow accurate tracking of the desired trajectories for the moderate ramp speed variations. A close link between the active q currents and the real power (torque), as well as the magnetizing d currents and Q, is immediately visible from the respective waveforms. The coupling effects of the i_{sq} clearly manifest themselves as speed (torque) dependent disturbance (e.g. offsets) in the

respective non-controllable i_{pd} profiles by analogy to the P and Q scenario in Fig. 4.
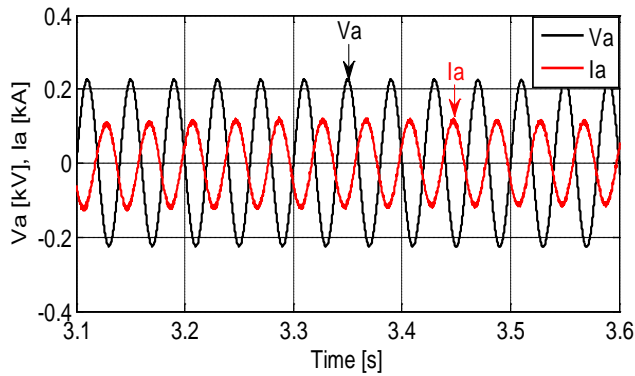

Fig. 7. Primary voltage and current at unity power factor.

Fig. 6 illustrates the step-wise PWM sector change of the modulated secondary voltage vector (v_s), and the respective current variations, during a speed reduction from 900 rev/min to 600 rev/min i.e. the speed mode change from super- to sub-synchronous. In the super-synchronous mode, v_s rotates anti-clockwise as indicated by the ascending sector numbers for the same phase sequence of the windings and $\omega_s > 0$ in (2). The situation is reversed at sub-synchronous speeds when v_s rotates clockwise with the sector numbers descending, which comes from the opposite phase sequence of the secondary to the primary winding since $\omega_s < 0$ in (2). Notice that v_s becomes stationary at synchronous speed as the secondary currents are then DC i.e. $\omega_s = 0$ in (2).

Finally, Fig. 7 shows the respective phase voltage and current waveforms which are π-rad out of phase as expected for unity power factor control (-1 in generating mode) in steady-state period.

VII. CONCLUSIONS

A novel maximum power factor control (MPFC) algorithm for optimum operation of the BDFRG – a viable, low cost and robust alternative to its widely-used counterpart, the conventional slip-ring doubly-fed induction generator (DFIG), has been introduced and evaluated by comprehensive simulation studies under typical operating conditions. Such vector control implementation can serve as a platform for further research on this emerging and prominent brushless machine topology for applications in large wind turbines, where the cost advantages of partially-rated power electronics and high reliability of brushless structure can be fully utilized.

The realistic simulation studies in Matlab®/Simulink® have clearly demonstrated the immense potential and effectiveness of the controller(s) using the maximum power factor control strategy. The presented results are more than encouraging and can serve as an incentive for further research on this machine.

REFERENCES

[1] M. G. Jovanovic, R. E. Betz, and J. Yu, "The use of doubly fed reluctance machines for large pumps and wind turbines," IEEE Transactions on Industry Applications, vol. 38, pp. 1508–1516, 2002.

[2] F.Wang, F.Zhang, and L.Xu, "Parameter and performance comparison of doubly-fed brushless machine with cage and reluctance rotors," IEEE Transactions on Industry Applications, vol. 38, no. 5, pp. 1237–1243, 2002.

[3] R. E. Betz and M. G. Jovanovic, "Introduction to the space vector modelling of the brushless doubly-fed reluctance machine," Electric Power Components and Systems, vol. 31, no. 8, pp. 729–755, 2003.

[4] D. G. Dorrell and M. Jovanovi´c, "On the possibilities of using a brushless doubly-fed reluctance generator in a 2 MW wind turbine," IEEE Industry Applications Society Annual Meeting, pp. 1–8, Oct. 2008.

[5] R.A.McMahon, P.C.Roberts, X.Wang, and P.J.Tavner, "Performance of BDFM as generator and motor," IEE Proc.-Electr. Power Appl., vol. 153, no. 2, pp. 289–299, March 2006.

[6] J. Poza, E. Oyarbide, I. Sarasola, and M. Rodriguez, "Vector control design and experimental evaluation for the brushless doubly fed machine," IET Electric Power Applications, vol. 3, no. 4, pp. 247–256, July 2009.

[7] K. Protsenko and D. Xu, "Modeling and control of brushless doubly-fed induction generators in wind energy applications," IEEE Transactions on Power Electronics, vol. 23, no. 3, pp. 1191–1197, May 2008.

[8] F. Valenciaga and P. F. Puleston, "Variable structure control of a wind energy conversion system based on a brushless doubly fed reluctance generator," IEEE Transactions on Energy Conversion, vol. 22, no. 2, pp. 499–506, June 2007.

[9] H. Polinder, F. van der Pijl, G. de Vilder, and P. Tavner, "Comparison of direct-drive and geared generator concepts for wind turbines," IEEE Transactions on Energy Conversion, vol. 21, no. 3, pp. 725–733, Sept. 2006.

[10] F. Spinato, P.J.Tavner, G. van Bussel, and E. Koutoulakos, "Reliability of wind turbine subassemblies," IET Renewable Power Generation, vol. 3, no. 4, pp. 387–401, Dec. 2009.

[11] S. Tohidi, M. Zolghadri, H. Oraee, P. Tavner, E. Abdi, and T. Logan, "Performance of the brushless doubly-fed machine under normal and fault conditions," IET Electric Power Applications, vol. 6, no. 9, pp. 621–627, Nov. 2012.

[12] F. Barati, R. McMahon, S. Shao, E. Abdi, and H. Oraee, "Generalized vector control for brushless doubly fed machines with nested-loop rotor," IEEE Transactions on Industrial Electronics, vol. 60, no. 6, pp. 2477–2485, June 2013.

[13] L. Xu, L. Zhen, and E. Kim, "Field-orientation control of a doubly excited brushless reluctance machine," IEEE Transactions on Industry Applications, vol. 34, no. 1, pp. 148–155, Jan/Feb 1998.

[14] A. Knight, R. Betz, and D. Dorrell, "Design and analysis of brushless doubly fed reluctance machines," IEEE Transactions on Industry Applications, vol. 49, no. 1, pp. 50–58, Jan/Feb 2013.

[15] T. Long, S. Shao, P. Malliband, E. Abdi, and R. McMahon, "Crowbar-less fault ride-through of the brushless doubly fed induction generator in a wind turbine under symmetrical voltage dips," IEEE Transactions on Industrial Electronics, vol. 60, no. 7, pp. 2833–2841, 2013.

[16] R. Cardenas, R. Pena, S. Alepuz, and G. Asher, "Overview of control systems for the operation of DFIGs in wind energy applications," IEEE Transactions on Industrial Electronics, vol. 60, no. 7, pp. 2776–2798, 2013.

[17] G. Marques and D. Sousa, "Understanding the doubly fed induction generator during voltage dips," IEEE Transactions on Energy Conversion, vol. 27, no. 2, pp. 421–431, 2012.

[18] S. Tohidi, P. Tavner, R. McMahon, H. Oraee, M. Zolghadri, S. Shao, and E. Abdi, "Low voltage ride-through of DFIG and brushless DFIG: Similarities and differences," Electric Power Systems Research, vol. 110, no. 0, pp. 64–72, 2014.

[19] T. Long, S. Shao, E. Abdi, R. McMahon, and S. Liu, "Asymmetrical low-voltage ride through of brushless doubly fed induction generators for the wind power generation," IEEE Transactions on Energy Conversion, vol.28, no.3, pp.502–511, 2013.

[20] E. Tremblay, S. Atayde, and A. Chandra, "Comparative study of control strategies for the doubly fed induction generator in wind energy conversion systems: A DSP-based implementation approach," IEEE Transactions on Sustainable Energy, vol. 2, no. 3, pp. 288–299, 2011.

[21] M. Jovanovic, "Sensored and sensorless speed control methods for brushless doubly fed reluctance motors," IET Electric Power Applications, vol. 3, no. 6, pp. 503–513, 2009.

[22] M. G. Jovanovi´c, J. Yu, and E. Levi, "Encoderless direct torque controller for limited speed range applications of brushless doubly fed reluctance motors," IEEE Transactions on Industry Applications, vol. 42, no. 3, pp. 712–722, 2006.

[23] H. Chaal and M. Jovanovi´c, "Practical implementation of sensorless torque and reactive power control of doubly fed machines," IEEE Transactions on Industrial Electronics, vol. 59, no. 6, pp. 2645–2653, 2012.

[24] H. Chaal and M. Jovanovic, "Power control of brushless doubly-fed reluctance drive and generator systems," Renewable Energy, vol. 37, no. 1, pp. 419–425, 2012.

[25] F. Valenciaga, "Second order sliding power control for a variable speed-constant frequency energy conversion system," Energy Conversion and Management, vol. 52, no. 12, pp. 3000–3008, 2010.

[26] R. E. Betz and M. G. Jovanovic, "Theoretical analysis of control properties for the brushless doubly fed reluctance machine," IEEE Transactions on Energy Conversion, vol. 17, pp. 332–339, 2002.

[27] M. Malinowski, M. Kazmierkowski, and A. Trzynadlowski, "A comparative study of control techniques for PWM rectifiers in ac adjustable speed drives," IEEE Transactions on Power Electronics, vol. 18, no. 6, pp. 1390–1396, 2003.

[28] S. Ademi, M. Jovanovic and J.K. Obichere, "Comparative analysis of control strategies for large doubly-fed reluctance wind generators," Proceedings of the World Congress on Engineering and Computer Science 2014 vol. 1 WCECS 2014, 22-24 October, 2014, San Francisco, USA.

[29] S. Ademi and M. Jovanovic, "Control of emerging brushless doubly fed reluctance wind turbine generators," in Large Scale Renewable Power Generation, ser. Green Energy and Technology, J. Hossain and A.Mahmud, Eds.Springer Singapore, 2014,pp.395–411.

[30] S. Ademi and M. Jovanovic, "Vector control methods for brushless doubly fed reluctance machines," IEEE Transactions on Industrial Electronics, vol. 62, no. 1, pp. 96-104, January, 2015.

[31] S. Ademi and M. Jovanovic, "High-efficiency control of brushless doubly-fed machines for wind turbines and pump drives," Energy Conversion and Management, vol. 81, pp. 120-132, May 2014.

[32] S. Ademi, M. Jovanovic and M. Hassan, "Control of brushless doubly-fed reluctance generators for wind energy conversion systems," IEEE Transactions on Energy Conversion, vol. PP, pp. 1-9, Feb 2015.